Large Eddy Simulation of Turbulent Combustion using Adaptive Mesh Refinement in a typical Micro Gas Turbine Combustor

Antoine VERHAEGHE[1]*, **Alessio PAPPA**[1], **Ward DE PAEPE** [1], **Pierre BENARD**[2], **Laurent BRICTEUX**[1]

[1]University of Mons, Polytechnic Faculty, Mechanical Department, 7000 Mons, Belgium
[2]Normandie University, INSA Rouen, UNIROUEN, CNRS, CORIA, Rouen 76000, France
*(Corresponding author: antoine.verhaeghe@umons.ac.be)

Abstract - This work aims at assessing an LES adaptive mesh refinement method on a specific test case: a typical industrial mGT burner. Dynamic adaptive mesh refinement allows to refine automatically, over time, regions of interest in the mesh, i.e. the flame zone for combustion applications. By comparing with an user-made mesh, the mesh adaptation provides a more accurate flame resolution without significantly increasing the computational cost.

Nomenclature

AMR	Adaptive Mesh Refinement	S	Flame Sensor
CHP	Combined Heat and Power	$TFLES$	Thickened Flame model for LES
CFL	Courant-Friedrich-Levy	Y	Mass Fraction
EGR	Exhaust Gas Recirculation	*Greek symbols*	
LES	Large Eddy Simulation	ϵ	Relative metric error
mGT	micro Gas Turbine	$\dot{\omega}$	Source term
M	Metric, mm		

1. Introduction

Accurate simulation of combustion is critical to assess the performances and emissions of a gas turbine combustor, as well as to identify possible issues or instabilities. In a context of global energy transition towards cleaner and more efficient decentralized power generation, small-scale combined heat and power production (CHP) units, such as micro Gas Turbines (mGTs), have to become more fuel and operational flexible. Several advanced cycle concepts have been studied and proven effective to enhance the flexibility of mGTs in CHP. Nevertheless, for all of these cycles, the combustion chamber is currently the limiting factor to implement these advanced cycle modifications, withholding the exploitation of their full potential. The combustion chamber must work under unconventional diluted conditions, such as Exhaust Gas Recirculation (EGR) — to perform carbon capture — or humidification — to allow to decouple heat and electric production by increasing the electrical efficiency and while doing so, also the profitability —, or must burn alternative fuels, i.e. Electro-fuels (E-fuels) — such as green hydrogen coming from the electrolysis of the excess renewable production — and Bio-fuels (such as syngas), while still ensuring flame stability, performances and low emissions.

To investigate the impact of such advanced cycle modifications or the use of different fuels on the combustion process, Large Eddy Simulation (LES) is a powerful tool. Indeed, LES can provide details of unsteady flow structures and can predict possible instabilities, known to be critical in many industrial practical applications. However, LES, still being rather limited to academic cases, remains challenging for real industrial applications. Indeed, the accuracy
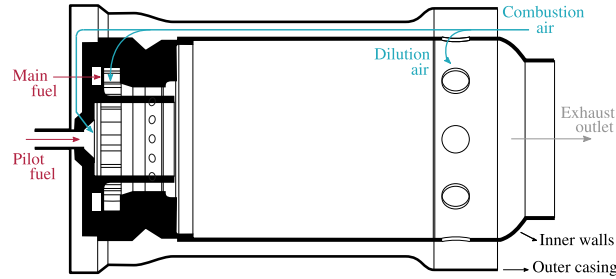
Figure 1: *The Turbec T100 combustion chamber is a reverse (or counter-current) flow can burner where the combustion air is entering between the outer casing and the inner walls of the combustor. The air reaches then the dilution holes, the pilot and main injectors by passing on the external surface of the inner walls.*

and quality of LES strongly depends on the mesh size. Therefore, performing LES induces a high computational cost due to the required heavy grids for complex industrial applications, like mGT combustors. Moreover, the mesh generation might be complex, especially when the regions of interest are not intuitively known.

An innovative solution to simplify mesh generation and to reduce computational cost lies in dynamic Adaptive Mesh Refinement (AMR). This technique consists in automatically refining the mesh all along the computational process, in the region of interesting quantities, according a physical criterion (turbulence, gradients, heat release, ...). Dynamic AMR features several advantages compared to a classical static refined mesh, such as: less prior knowledge needed of the solution during the meshing phase; significant less meshing time and human effort before the simulation; and finally, it allows to generate lighter meshes with less computational elements in the zones where there is no key physical quantities, reducing theoretically the computational cost while maintaining or even improving the results accuracy [1].

However, LES of combustion with dynamic AMR has only been tested on academic cases with simple geometries and relatively light meshes. Therefore, the objective of this work is to investigate the application of AMR for LES of a complex industrial geometry to capture the combustion more accurately without significantly increasing the computational cost. In this respect, a dynamic AMR method will be implemented on the LES of a typical industrial mGT burner, namely the Turbec T100 mGT combustor. The paper is organized as follow: a description of the test case set-up, then the computational approach methodology, and finally the results where the methodology is assessed on the test case for different AMR strategies.

2. T100 mGT Combustor

The considered mGT combustor has been inspired on the combustion chamber of the Turbec T100 mGT [2] which features a can swirl burner layout (Fig. 1). The particularly challenging mesh generation for industrial gas turbine combustors, due to the geometrical complexity, requires simplification with respect to the actual geometry. Therefore, the complex geometry of the original burner (Fig. 1) has been adapted to a simplified cylindrical layout, as presented in Fig. 2. Despite the simplifications, this generic geometry still conserves and represents the main features of the actual chamber, while offering flexibility, as well as allowing to assess the general trends required by the main goal of the previous works of the authors [3]. More details about characteristics of the simplified combustion chamber can be found in [3]. Similar operating conditions as for the T100, reported in Table 1, have been considered in this work.
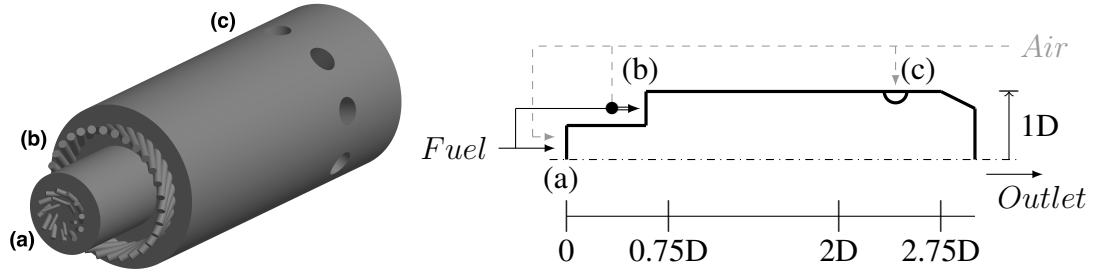
Figure 2: *3D and 2D representations of the simulation domain defined by the inner walls of the combustion chamber (Fig. 1) where the total combustion air flow rate is distributed as follows: 4% in the 12 pilot injectors for air (and 6 for fuel) for the diffusion pilot flame (a), 21% in the 30 main premixed injectors (b) and 75% through the 9 dilution holes (c).*

	Typical mGT case
Total air mass flow rate [g/s]	690
Pilot fuel injector mass flow rate [g/s]	1
Main fuel injector mass flow rate [g/s]	5.5
Pressure [bar]	4
Fuel inlet temperature [K]	300
Air inlet temperature [K]	865
Thermal power [kW]	325
Overall equivalence ratio [.]	0.163
Fuel mass fraction Y_{fuel}	100% CH_4
Combustion air mass fraction Y_{air}	76.79% N_2 / 23.21% O_2

Table 1: *Operating conditions of the generic combustion chamber representative for operation at nominal power of the actual combustor of the Turbec T100.*

3. Computational approach

3.1. Numerical set-up

Large Eddy simulations were performed using the massively parallel flow solver YALES2 [4]. This finite-volume code solves the low-Mach number Navier-Stokes equations using a projection method for variable density flows. Equations are solved using a 4th order centered scheme in space and a 4th order Runge-Kutta-like scheme in time. The turbulent sub-grid scale stresses are modelled with the local dynamic Smagorinsky model. The stability of the time integration is ensured with an adaptive time step that keeps the maximum local CFL number under 0.4. A classical log-law profile is used as wall model. Moreover, adiabatic walls condition is considered (no heat losses). The LES of the combustion are performed coupling finite-rate chemistry to a detailed chemical mechanism. The conservation equations for reacting flows (mass, species, momentum and energy) are solved by transporting all species of the chemical mechanism and evaluating the source terms from the kinetic mechanism. The kinetic scheme DRM19 (21 species and 84 reactions) is used in our LES [5]. The dynamic Thickened Flame model (DTFLES) is used to model the sub-grid scale turbulence/chemistry interaction on the LES grid [6]. The flame thickening is locally activated in regions identified by the flame sensor. This flame sensor is based on the species source term $\dot{\omega}_C$, which depends on reaction products: $\dot{\omega}_C = \dot{\omega}_{CO_2} + \dot{\omega}_{CO} + \dot{\omega}_{H_2O}$. The flame sensor is set to 1 when $\dot{\omega}_C$ exceeds 10% of its maximal value for a 1D laminar flame in the same operating conditions. The use of the DRM19

mechanism and of the DTFLES model has been validated in previous works [7].

3.2. Adaptive Mesh Refinement

The AMR process involves imposing a target metric in some mesh regions according to a user-defined criterion. This criterion must allow to identify the zones of interest in the mesh. For combustion applications, regions of interest correspond to the flame front where most of chemical reactions occur. Therefore, the flame sensor S, aiming to identify the flame front for the TFLES model, can be used as mesh adaptation criterion. Hence, regions of interest are identified as regions in which the flame sensor is not zero. Then two target metrics have to be specified: the target metric in the flame front, called the front metric, and the target metric in non-reactive regions, i.e the regions outside the flame front, called the background metric. The front metric is defined as a constant and the background metric can be defined in two ways: either by imposing a constant metric value, or by keeping the metric of the initial mesh. The transition between cells in the flame front and in background region is driven by a fixed maximum cell size gradient.

The highly turbulent character of the combustion process involves a random flame front displacement over time in the combustion chamber. Therefore, the mesh has to be adapted over time to match the target metric with the flame front location. In this respect, it is necessary to define when the adaptation will be triggered during the simulation. To this end, the approach used consists in triggering mesh adaptation when the mesh metric deviates from the target metric. With this in mind, the relative metric error is defined:

$$\epsilon = \max \left(\left| \frac{M_{current} - M_{target}}{M_{target}} \right| \right), \tag{1}$$

where $M_{current}$ and M_{target} are respectively the current cell metric and the target cell metric. The adaptation process is triggered when this relative error exceeds a maximum acceptable error ϵ_{max} set at 200% in this work. The main advantage of this method is that it is based on a numerical indicator and not a physical one. Therefore, the mesh adaptation does not depend on the flow dynamics and can treat combustion in the same way under different diluted conditions, allowing for future works to integrate advanced cycles such as humidification, Exhaust Gas Recirculation (EGR) or alternative fuels combustion such as hydrogen.

4. Results

Adaptive Mesh Refinement (AMR) has been applied to the mGT combustor configuration, starting from a reference case [3], with a mesh size of about 33 millions of elements. Two AMR cases were considered: for the first case (AMR1) a $1\,\mathrm{mm}$ metric is set in the flame front and a $5\,\mathrm{mm}$ constant background metric in other regions, while for the second case (AMR2) a $1\,\mathrm{mm}$ metric is set in the flame region but the initial REF mesh is conserved in the background zone. Meshes obtained for both cases, compared to the initial mesh, captured at one specific moment are shown in Fig. 3. For both cases, simulations ran collecting statistics over 3 convective times.

4.1. Qualitative analysis

The flame sensor maps, used to identify the flame location, are superimposed to the meshes of the 3 cases in Fig. 3. For the REF case, we can clearly observe that the flame, characterized by a flame sensor value larger than zero (red color), extends outside the refined zone, especially close to the wall. It demonstrates that the predefined regions in the reference mesh are not large
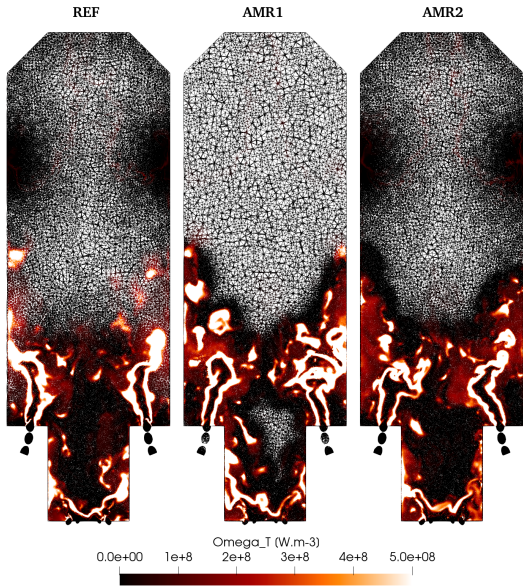
Figure 3: *Comparison of the instantaneous reaction rate fields, superposed to the mesh, in a 2D cross section plan along the axial axis, highlight that in the REF case (left) the flame extends beyond the predefined refined zone, while in both AMR1 (center) and AMR2 (right), the mesh is refined around the flame.*
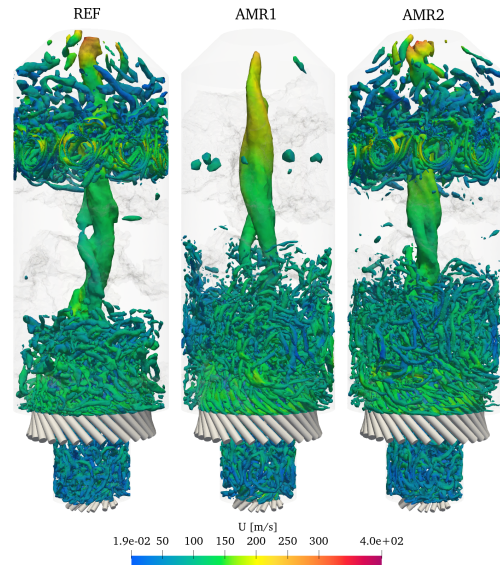

Figure 4: *Iso-contours of Q-criterion at value $Q = 5 * 10^7$ s^2 coloured by the velocity for the REF (left), AMR1 (center) and AMR2 (right) cases show that the AMR2 case provides as much details as AMR1 case in the flame area, but still allows to capture the turbulence generated by the dilution holes as for REF case.*

enough to encompass the flame. In contrast, the flame is well contained within the refined zone for both AMR cases. In addition, we can observe that the geometry of the refined zone in the AMR cases correspond to the shape of the flame. This refined zone is nevertheless enlarged to ensure a safety margin. Indeed, the number of propagation cells N_p has been set at 7. This safety margin allows to compensate metric errors close to 200% while ensuring that the flame is enclosed within the refined mesh. Note that the values of the parameters ϵ_{max} and N_p have been mutually determined to correctly capture the flame along the simulation while ensuring a reasonable computational cost.

The turbulent flow resolution in the combustion chamber can be qualitatively assessed by using the Q-criterion which allows to visualize resolved turbulent structures [4]. As shown in Fig. 4, the swirl injection induces the production of turbulent structures in the pilot and main flame regions for the 3 cases. However, both AMR cases present more observable vortical structures near the combustor walls and in the flame diffusion zone compared to the reference case due to a finer mesh resolution in these regions. Then, near the dilution holes at the combustor outlet, highly turbulent motions are observed for the reference and AMR2 cases, while almost none of these structures are resolved for the AMR1 case owing to a too poor mesh resolution in this region. Indeed, this zone without combustion has been automatically de-refined for the AMR1 case.
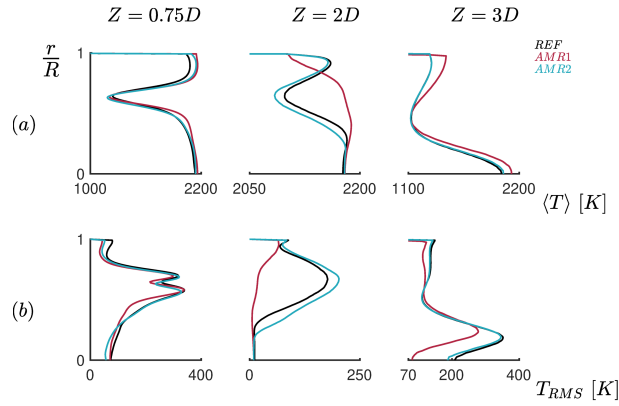
Figure 5: *Comparison of azimuthal time average (a) and RMS (b) temperature between the reference (in black), AMR1 (in blue) and AMR2 (in red) cases in 3 positions taken along the combustion chamber: Z=0.75D, Z=2D and Z=2.75D, demonstrating the benefits of applying AMR in the flame region.*

4.2. Quantitative analysis

To confirm the observed trends in the qualitative analysis, a quantitative comparison of temperature and reaction rate profiles has been performed at 3 axial positions along the combustion chamber (Fig. 2): in the flame region (Z=0.75D), before the dilution holes (Z=2D) and close to the outlet (Z=2.75D). Fig. 5 shows the azimuthal time average and RMS temperature profiles for the 3 cases.

Regarding the temperature, we can observe that the 3 profiles are similar in the flame region (Z=0.75D Fig. 5 (a)). Nevertheless, slightly higher temperatures are observed close to the wall for the AMR cases (difference of $100\,^{\circ}\mathrm{C}$ representing an increase of $5\,\%$). Indeed, for both AMR cases, the mesh is refined in this region when the flame propagates along the wall, while the REF case presents a coarser mesh in this zone. Therefore, the temperature is more accurately predicted in both AMR cases close to the wall. Before the dilution holes (Z=2D), we can notice two different profile trends: for the AMR1 case, the temperature is maximal at the center of the combustion chamber and decreases when approaching the wall, while, for the REF and AMR2 cases, the minimal temperature is observed at a certain distance from the wall. This difference can be explained by the fact that the more refined REF and AMR2 meshes allow to capture correctly the cold air flow entering the combustion chamber through the dilution holes compared to the AMR1 case. At the outlet of the combustion chamber (Z=2.75D), the AMR1 profile presents higher temperatures and lower fluctuations than both other cases. Moreover, the average temperature at the outlet are 1244K for the REF case, 1302K for the AMR1 case and 1244K for the AMR2 case. This clearly highlights that the dilution effect of flue gas by cold air is not properly captured by the AMR1 mesh, leading to an overestimation of the outlet temperature.

The mass fractions of the CO_2 and CO emissions at the outlet of the combustion chamber are reported in Table 2. The CO_2 and CO emissions are similar for the REF and AMR2 cases, while higher emissions are observed for the AMR1 case, showing the strong influence of the mesh on the emissions calculation. Indeed, in the combustion region, the mesh size, and thus the thickening factor, have an impact on the species production and more especially on intermediate species, such as CO, as highlighted by Bénard et al. [8]. Then, at the outlet, the effect of the air dilution is less accurately captured with the coarser the mesh (AMR1 case), resulting in higher CO_2 and CO concentrations.

4.3. Computational cost

This section presents a comparison of computational resources used between the REF, AMR1 and AMR2 cases (Table 3). The simulation were performed on the Zenobe cluster [9]. The adapted grid AMR1 contains a lower number of cells than the reference mesh due to de-refining in non-combustion areas, while the AMR2 mesh has a slightly higher number of cells than the reference mesh. The reduced number of cells in the AMR1 mesh has the advantage of requiring less computing cores compared to the other two cases. Moreover, as shown in Table 3, the mesh adaptation has an influence on the mean time step, especially for the AMR1 case. Indeed, the limiting cells, which set the time step, are located around the dilution holes for the REF and the AMR2 cases because of the fine mesh and the high flow velocity in this zone. Whereas the limiting cells for the AMR1 case are located in the main injector because the mesh is coarser around dilution holes, which explains the higher average time step. Regarding the CPU cost, the AMR1 and AMR2 cases are respectively 17% and 70% more expensive than the reference case, highlighting the high cost of dynamic mesh adaptation. Indeed, the mesh adaptation contributes, respectively for the AMR1 and AMR2 cases, to 33% and 15% of the total CPU cost.

5. Conclusions

This paper presents a dynamic adaptive mesh refinement methodology for LES of a typical industrial mGT combustor. The mesh adaptation is based on a flame sensor criterion allowing to identify combustion regions. The mesh adaptation triggering is based on the relative metric error, representing the deviation from the target metric. Starting from an initial mesh, refined according to the experience of the users, two different AMR strategies have been compared. The first implies the refinement in combustion regions and the de-refining of other zones, while the second considers the refinement in the flame region but keep the reference mesh in non-combustion regions. The results show obviously a more accurate combustion resolution in the flame region for both AMR cases compared to the reference case. However, the de-refining of non-combustion regions leads to a less accurate resolution of the flue gas dilution at the outlet of the combustion chamber, overestimating outlet emissions and temperature. Regarding the computational cost, although this mesh is by average 40% lighter than the reference mesh, the total CPU cost is 17% higher due to the significant cost of mesh adaptation. The second case, keeping the initial mesh in background and, thus, containing a slightly higher number of cells than the reference mesh, is 70% more expensive.

In summary, adaptive mesh refinement allows to generate automatically a quality mesh in region of interest, i.e. in the flame zone, reducing significantly human effort but increasing computational cost. However, the computational cost can be lowered by reducing the resolution in the dilution region if an accurate prediction of emissions is not required.

	REF	AMR1	AMR2
Y_{CO_2}	2.57 %	2.99 %	2.56 %
Y_{CO}	34 ppm	48 ppm	35 ppm

Table 2: *Time and space average of the mass fractions emissions of the CO_2 and CO at the outlet of the combustion chamber for reference and AMR cases, highlighting the negative impact on emission prediction of using a coarse mesh in the dilution region.*

.

	REF	AMR1	AMR2
Mean number of mesh elements [Millions]	33.1	19.6	34.5
Mean number of mobilized cores	662	360	697
Mean time step [µs]	0.28	0.41	0.35
Total CPU cost for $1\,\text{ms}$ [kCPUh]	3.18	3.73	5.44
Mesh adaptation CPU cost for $1\,\text{ms}$ [kCPUh]	0	1.24	0.83
Mesh adaptation CPU cost/ Total CPU cost [%]	0	33.1	15.24

Table 3: *Computational performances for reference and both AMR cases, illustrating the high cost of mesh adaptation.*

References

[1] P. Bénard, G. Balarac, V. Moureau, C. Dobrzynski, G. Lartigue, Y. D'Angelo, Mesh adaptation for large-eddy simulations in complex geometries, International Journal for Numerical Methods in Fluids 81 (12) (2016) 719–740.

[2] Turbec, T100 microturbine CHP system: Technical description version 4.0 (2010-2011).

[3] A. Pappa, B. Bricteux, P. Bénard, W. De Paepe, Can water dilution avoid flashback on a hydrogen enriched micro gas turbine combustion? — a large eddy simulations study, Journal of Engineering for Gas Turbine and Power 143 (2020) 041008.

[4] V. Moureau, P. Domingo, L. Vervisch, Design of a massively parallel CFD code for complex geometries, Comptes Rendus Mecanique 339 (2-3) (2011) 141–148.

[5] A. Kazakov, M. Frenklach, DRM19 mechanism.

[6] O. Colin, F. Ducros, D. Veynante, T. Poinsot, A thickened flame model for large eddy simulations of turbulent premixed combustion, Physics of Fluids 12 (7) (2000) 1843–1863.

[7] A. Pappa, M. Cordier, P. Bénard, L. Bricteux, W. De Paepe, How do water and co2 impact the stability and emissions of the combustion in a micro gas turbine? — a large eddy simulations comparison, Energy 248 (2022) 123446.

[8] P. Bénard, G. Lartigue, V. Moureau, R. Mercier, Large-eddy simulation of the lean-premixed preccinsta burner with wall heat loss, Proceedings of the Combustion Institute 37 (4) (2019) 5233 – 5243.

[9] C. C. des Equipements de Calcul Intensif, [Consulted on 30/04/2020]. [link].
URL http://www.ceci-hpc.be/clusters.html

Acknowledgements